

The various architectures and properties of a series of coordination polymers tuned by the central metals†

Cite this: *Dalton Trans.*, 2014, **43**, 8072

Xiu-Li Wang,* Jian Luan, Hong-Yan Lin, Mao Le and Guo-Cheng Liu

Five new metal–organic coordination polymers based on the mixed ligands of a semi-rigid bis-pyridyl-bis-amide *N,N'*-bis(3-pyridinecarboxamide)-1,2-cyclohexane (3-bpah) and 1,4-benzenedicarboxylic acid (1,4-H₂BDC), namely [Co(3-bpah)(1,4-BDC)(H₂O)₃] (**1**), [Ni(3-bpah)(1,4-BDC)(H₂O)₃] (**2**), [Cu(3-bpah)(1,4-BDC)] (**3**), [Zn(3-bpah)(1,4-BDC)]·H₂O (**4**) and [Cd(3-bpah)(1,4-BDC)(H₂O)] (**5**), have been hydrothermally synthesized and structurally characterized. Complexes **1** and **2** are isostructural and display the similar 1D infinite chains, which are further linked *via* hydrogen-bonding interactions to generate 3D supramolecular frameworks. Complex **3** features a 3D polymeric framework with CdSO₄-like topology. Complexes **4** and **5** show two similar 2D (2,4)-connected networks with (4-8⁵)(4) topology, in which the 3-bpah ligands adopt different μ₂-bridging coordination modes *via* the ligation of two pyridyl nitrogen atoms in **4** and *via* the ligation of one pyridyl nitrogen and one amide oxygen atom in **5**. In addition, the central metals show different coordination geometries in **4** and **5**. The adjacent layers of complexes **4** and **5** are finally extended into 3D supramolecular architectures through hydrogen-bonding interactions. The effects of the central metals on the structures and properties of complexes **1–5** have been discussed. The electrochemical properties of complexes **1–3** and fluorescent sensing behaviors of **4–5** toward ethanol and nitrobenzene have been investigated in detail.

Received 8th January 2014,
Accepted 26th February 2014

DOI: 10.1039/c4dt00064a

www.rsc.org/dalton

Introduction

The design and synthesis of novel metal–organic coordination polymers (MOCs) using crystal engineering concepts have become increasingly popular during the past few decades.^{1–4} These novel and various networks possess a wide range of properties, which make them potential materials for applications in luminescence, electrochemistry, catalysis, magnetism, gas storage and separation.^{5–12} Typically, luminescent and electrochemical materials have been extensively explored for their diverse functionalities and applications in lighting, display, sensing, electrocatalysis and optical devices.^{13–17} The suitable selection of metal ions is one of the most important prerequisites for constructing MOCs with luminescent and electrochemical properties, and a large number of such MOCs have been synthesized.^{13–17} For example, the Zn/Cd ions are the most commonly reported and are widely used to construct luminescent MOCs because the d¹⁰ metal ions not only possess various coordination numbers, but also show excellent

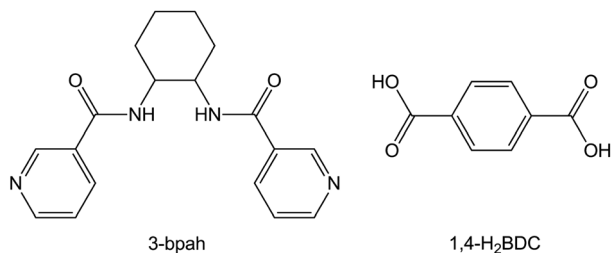
luminescent properties when coordinated by multidentate ligands.^{18,19} Li's group has reported two Zn-based MOCs with a 1D channel through multi-component self-assembly at room temperature, namely {[Zn(OCA-OH)₂(4,4'-bipy)_{0.5}]}·1.67H₂O)_n (OCA-OH = (*E*)-3-(2-hydroxyl-phenyl)-acrylic acid; 4,4'-bipy = 4,4'-bipyridine) and {[Zn(MCA-OH)₂(4,4'-bipy)_{0.5}]}·0.5CH₃OH·H₂O)_n (MCA-OH = (*E*)-3-(3-hydroxyl-phenyl)-acrylic acid). Their guest-free forms demonstrate their potential as a potential luminescent probe or sensor for small molecules, and the MOCs also show exceptional fluorescence quenching and enhancement behaviors for different types of aromatic molecules.²⁰ In addition, various efforts have been made to study the electrochemical and electrocatalytic activities of MOCs with Co(II)/Ni(II)/Cu(II) ions.^{16,17} From the synthesis point of view, Co(II)/Ni(II)/Cu(II)-containing MOCs have attracted significant interest in both the scientific and industrial fields because of their low background current, easy fabrication and good performance.^{16,17} Benvidi and co-workers prepared a Co(II) bis(benzoylacetone)ethylenediimino multi-wall carbon nanotube modified carbon paste electrode (Co(II) L-MWCNT-CPE), which was applied to the determination of hydroxylamine in water and pharmaceutical samples.²¹

Recently, our group has been working on the syntheses of transition metal complexes containing rigid/semi-rigid/flexible bis-pyridyl-bis-amide ligands, and a series of coordination

Department of Chemistry, Bohai University, Jinzhou, 121000, P. R. China.

E-mail: wangxiuli@bhu.edu.cn; Fax: +86-416-3400158; Tel: +86-416-3400158

† Electronic supplementary information (ESI) available: IR spectra, TG and additional figures. CCDC numbers 962356–962360. For ESI and crystallographic data in CIF or other electronic format see DOI: 10.1039/c4dt00064a



Scheme 1 The semi-rigid bis-pyridyl-bis-amide *N,N'*-bis(3-pyridinecarboxamide)-1,2-cyclohexane (3-bpah) and 1,4-benzenedicarboxylic acid (1,4-H₂BDC) used in this work.

polymers with various properties have been constructed.^{22–24} As a continuation of our previous study, in this contribution, five transition metal ions (Co(II), Ni(II), Cu(II), Zn(II), Cd(II)) were selected as the central metals, and a semi-rigid bis-pyridyl-bis-amide ligand *N,N'*-bis(3-pyridinecarboxamide)-1,2-cyclohexane (3-bpah) and 1,4-benzenedicarboxylic acid (1,4-H₂BDC) have been used as the mixed ligands (Scheme 1), to constructing novel MOCs with good luminescent sensing or electrochemical properties. We investigated the effect of the metal ions on the structures and properties of the title complexes. As a result, five new MOCs with different dimensionalities, namely [Co(3-bpah)(1,4-BDC)(H₂O)₃] (1), [Ni(3-bpah)(1,4-BDC)(H₂O)₃] (2), [Cu(3-bpah)(1,4-BDC)] (3), [Zn(3-bpah)(1,4-BDC)]·H₂O (4) and [Cd(3-bpah)(1,4-BDC)(H₂O)] (5) have been obtained. The crystal structures of the five MOCs have been represented and discussed. The fluorescence properties of the coordination polymers 1–5, the fluorescent selectivities and fluorescent sensing behaviours of 4 and 5, and the electrocatalytic activities of 1–3 have been investigated in detail.

Experimental section

Materials and measurements

All reagents were obtained from commercial sources without further purification. The N-donor ligand 3-bpah was prepared according to the literatures.²⁵ The elemental analyses (C, H and N) were determined on a Perkin-Elmer 240C elemental analyzer. The FT-IR spectra (KBr pellets) were taken on a Varian 640-IR spectrometer in the range of 500–4000 cm⁻¹. Powder XRD investigations were carried out with an Ultima IV with a D/teX Ultra diffractometer at 40 kV, 40 mA with Cu Kα (λ = 1.5406 Å) radiation. The thermogravimetric data for the complexes 1–5 were obtained using a Pyris Diamond thermal analyzer. The fluorescence spectra were recorded at room temperature on a Hitachi F-4500 fluorescence/phosphorescence spectrophotometer. A CHI 440 electrochemical workstation connected to a Digital-586 personal computer was used for the control of the electrochemical measurements and for data collection. A conventional three-electrode cell was used at room temperature. The carbon paste electrodes bulk-modified with complexes 1–3 (1-CPE, 2-CPE, 3-CPE) were used as the working electrodes. An SCE (saturated calomel electrode) and

a platinum wire were used as the reference and auxiliary electrodes, respectively.

X-ray crystallographic study

The X-ray diffraction data for complexes 1–5 were collected on a Bruker SMART APEX II diffractometer equipped with a CCD area detector and graphite-monochromated Mo Kα (λ = 0.71073 Å) by the ω and θ scan mode at 296(2) K. All of the structures were solved by direct methods and refined on *F*² by full-matrix least-squares methods using the SHELXS program of the SHELXTL package.²⁶ For complexes 1–5, the crystal parameters, data collection and refinement results are summarized in Table 1. Selected bond distances and bond angles are listed in Table S1–S5.† The hydrogen-bonding geometries of complexes 1, 4 and 5 are summarized in Table S6.†

The preparation of the title complexes

The synthesis of [Co(3-bpah)(1,4-BDC)(H₂O)₃] (1). A mixture of CoCl₂·6H₂O (0.048 g, 0.2 mmol), 3-bpah (0.032 g, 0.10 mmol), 1,4-H₂BDC (0.025 g, 0.15 mmol) and NaOH (0.016 g, 0.40 mmol) in 12 mL water was stirred for 30 min at room temperature, transferred to a 25 mL Teflon-lined autoclave and kept at 120 °C for 4 days. After slowly cooling to room temperature, pink block-shaped crystals of 1 suitable for X-ray diffraction were obtained (yield: 27% based on Co). If the molar ratio of the reactance was changed to 1 : 1 : 1, the yield is up to 55% (based on Co). Anal. calcd for C₂₆H₃₀CoN₄O₉: C 51.87, H 4.99, N 9.31. Found: C 51.83, H 4.95, N 9.37%. ν_{max} (KBr)/cm⁻¹: 3300 (m), 3079 (m), 2935 (w), 1649 (s), 1598 (s), 1549 (s), 1482 (m), 1422 (m), 1364 (s), 1326 (m), 1292 (m), 1218 (w), 1199 (w), 1145 (w), 1119 (w), 1053 (w), 931 (w), 862 (w), 755 (s), 698 (s), 644 (m), 598 (w), 514 (w).

The synthesis of [Ni(3-bpah)(1,4-BDC)(H₂O)₃] (2). Complex 2 was prepared in the same way as 1, except that NiCl₂·6H₂O (0.048 g, 0.2 mmol) was used instead of CoCl₂·6H₂O. Green block-shaped crystals of 2 suitable for X-ray diffraction were obtained (yield: 29% based on Ni). If the molar ratio of the reactance was changed to 1 : 1 : 1, the yield is up to 63% (based on Ni). Anal. calcd for C₂₆H₃₀N₄NiO₉: C 51.89, H 4.99, N 9.31. Found: C 51.93, H 5.01, N 9.30%. ν_{max} (KBr)/cm⁻¹: 3299 (m), 3083 (w), 2936 (w), 1649 (s), 1599 (s), 1550 (s), 1483 (m), 1422 (m), 1365 (s), 1325 (m), 1237 (w), 1199 (w), 1145 (w), 1119 (w), 1092 (w), 1050 (w), 930 (w), 868 (w), 814 (m), 755 (s), 698 (m), 598 (w), 513 (w).

The synthesis of [Cu(3-bpah)(1,4-BDC)] (3). The synthetic procedure for 3 was the same as for 1, except that CuCl₂·2H₂O (0.034 g, 0.2 mmol) was used instead of CoCl₂·6H₂O. Blue crystals of 3 suitable for X-ray diffraction were isolated by mechanical separation from the amorphous solid in 30% yield (based on Cu). If the molar ratio of the reactance was changed to 1 : 1 : 1, the yield is up to 47% (based on Cu). Anal. calcd for C₂₆H₂₄CuN₄O₆: C 56.52, H 4.35, N 10.14. Found: C 56.48, H 4.39, N 10.18%. ν_{max} (KBr)/cm⁻¹: 3525 (w), 2923 (w), 1651 (s), 1607 (s), 1562 (s), 1485 (s), 1431 (m), 1369 (s), 1309 (s), 1242 (w), 1198 (m), 1144 (m), 1090 (w), 1016 (w), 973 (w), 891 (w), 835 (m), 752 (s), 699 (s), 657 (m), 594 (m), 507 (w).

Table 1 The crystal data and structure refinement for complexes 1–5

Complex	1	2	3	4	5
Empirical formula	C ₂₆ H ₃₀ CoN ₄ O ₉	C ₂₆ H ₃₀ N ₄ NiO ₉	C ₂₆ H ₂₄ CuN ₄ O ₆	C ₂₆ H ₂₆ ZnN ₄ O ₇	C ₂₆ H ₂₆ CdN ₄ O ₇
Formula weight	601.47	601.25	552.03	571.88	618.91
Crystal system	Triclinic	Triclinic	Monoclinic	Triclinic	Triclinic
Space group	<i>P</i> $\bar{1}$	<i>P</i> $\bar{1}$	<i>C</i> 2/c	<i>P</i> $\bar{1}$	<i>P</i> $\bar{1}$
<i>a</i> (Å)	8.7946(5)	8.7723(3)	19.719(3)	9.3074(5)	7.8559(4)
<i>b</i> (Å)	12.8230(8)	12.7797(5)	9.0200(12)	11.8484(6)	11.5298(6)
<i>c</i> (Å)	13.5008(8)	13.4540(5)	16.077(2)	13.2041(6)	16.1232(8)
α (°)	76.2220(10)	76.1920(10)	90	108.8050(10)	82.5120(10)
β (°)	85.6630(10)	85.5170(10)	105.865(2)	97.7350(10)	81.0530(10)
γ (°)	72.7250(10)	72.7230(10)	90	112.4420(10)	73.3020(10)
<i>V</i> (Å ³)	1411.99(15)	1398.57(9)	2750.6(6)	1217.51(11)	1376.12(12)
<i>Z</i>	2	2	2	2	2
<i>D</i> /g cm ⁻³	1.415	1.428	1.33	1.560	1.494
μ /mm ⁻¹	0.666	0.752	0.839	1.065	0.843
<i>F</i> (000)	626	628	1140	592	628
Reflection collected	7133	7121	6765	6230	6984
Unique reflections	4921	4882	2418	4247	4824
Parameters	368	368	169	343	343
<i>R</i> _{int}	0.0077	0.0083	0.0265	0.0094	0.0086
GOF	1.047	1.063	1.020	1.038	1.020
<i>R</i> ₁ ^a [<i>I</i> > 2 σ (<i>I</i>)]	0.0451	0.0436	0.0559	0.0258	0.0211
<i>wR</i> ₂ ^b (all data)	0.1315	0.1273	0.1265	0.0756	0.0569

$$^a R_1 = \sum ||F_o| - |F_c|| / \sum |F_o|, \quad ^b wR_2 = \sum [w(F_o^2 - F_c^2)^2] / \sum [w(F_o^2)^2]^{1/2}.$$

The synthesis of [Zn(3-bpah)(1,4-BDC)]·H₂O (4). Complex 4 was synthesized with same procedure as for 1, using Zn(NO₃)₂·6H₂O (0.060 g, 0.2 mmol) in place of CoCl₂·6H₂O, leading to the formation of colorless block crystals of 4 (yield: 36% based on Zn). If the molar ratio of the reactance was changed to 1 : 1 : 1, the yield is up to 63% (based on Zn). Anal. calcd for C₂₆H₂₆ZnN₄O₇: C 54.56, H 4.55, N 9.79. Found: C 54.60, H 4.51, N 9.74%. ν_{\max} (KBr)/cm⁻¹: 3280 (m), 2943 (w), 1656 (s), 1601 (s), 1542 (s), 1475 (m), 1428 (m), 1402 (m), 1382 (s), 1354 (s), 1245 (w), 1208 (w), 1132 (m), 1092 (w), 1054 (m), 882 (w), 829 (s), 752 (s), 697 (s), 654 (w), 592 (w), 502 (w).

The synthesis of [Cd(3-bpah)(1,4-BDC)(H₂O)] (5). Complex 5 was synthesized with same procedure as for 1, using CdCl₂·2.5H₂O (0.045 g, 0.2 mmol) in place of CoCl₂·6H₂O, leading to the formation of colorless block crystals of 5 (yield: 28% based on Cd). If the molar ratio of the reactance was changed to 1 : 1 : 1, the yield is up to 57% (based on Cd). Anal. calcd for C₂₆H₂₆CdN₄O₇: C 50.41, H 4.20, N 9.05. Found: C 50.47, H 4.24, N 9.07%. ν_{\max} (KBr)/cm⁻¹: 3412 (m), 2939 (w), 1652 (s), 1624 (s), 1582 (s), 1502 (m), 1433 (s), 1367 (s), 1199 (w), 1141 (m), 1091 (w), 1018 (w), 886 (w), 834 (w), 778 (m), 744 (s), 646 (w), 541 (w).

The preparation of 1–3-CPE. The complexes 1–3 bulk-modified carbon paste electrodes (1-CPE, 2-CPE, 3-CPE) were fabricated by the following steps. Graphite powder 0.11 g and complex 1, 2 or 3 0.010 g were mixed together with an agate mortar for about 30 min to achieve a mixture; then 0.05 mL paraffin oil was added and stirred with a glass rod.²⁷ The homogenized mixture was packed into a 3 mm inner diameter glass tube, and a copper stick was used as the electrical contact. The surface of the modified electrodes was polished on a piece of weighing paper to achieve a mirror finish before use.

Results and discussion

Description of the structures

[Co(3-bpah)(1,4-BDC)(H₂O)₃] (1) and [Ni(3-bpah)(1,4-BDC)(H₂O)₃] (2). The single crystal X-ray structural analysis reveals that complexes 1 and 2 crystallize in the triclinic space group *P* $\bar{1}$, and they have an isostructural 3D supramolecular architecture based on a 1D polymeric chain [Co(3-bpah)(1,4-BDC)(H₂O)₃] and [Ni(3-bpah)(1,4-BDC)(H₂O)₃] (Fig. 1 and Fig. S1†). Therefore, complex 1 is employed as a representative structure to be described in detail. The structure of 1 contains two crystallographically unique Co(II) ions, as depicted in Fig. 1a. The Co1 ion takes a distorted octahedral geometry *via* coordinating to two pyridyl nitrogen atoms (N1 and N1#1) of 3-bpah and four oxygen atoms (O1W, O1W#1, O2W and O2W#1) of four coordination water molecules, whereas the octahedral Co2 center is coordinated by two pyridyl nitrogen atoms (N2 and N2#1) of 3-bpah and two oxygen atoms (O1, O1#1) of two 1,4-BDC anions plus two oxygen atoms (O3W, O3W#1) of coordination water molecules [Co–N = 2.174(2)–2.237(3) Å, Co–O = 2.0599(19)–2.0889(18) Å]. The adjacent Co1 and Co2 centers are alternately linked by the μ_2 -bridging 3-bpah (*via* ligation of two pyridyl nitrogen atoms, Table S7†) ligands to form a 1D [Co(3-bpah)]_n *meso*-helical chain (Fig. 1b), the non-bonding Co1...Co2 distance is 10.67 Å. Then, each 1,4-BDC anion acting as a monodentate ligand coordinates to the Co2 ion through only one carboxylic oxygen atom, leaving the other oxygen atoms non-coordinated and resulting in a fish-bone chain (Fig. S2a†). The hydrogen-bonding interactions between the coordinated water molecules and the carboxyl oxygen atoms O1W–H1WA...O4 (2.7023 Å) are found to assemble these 1D chains into a 2D layer (Fig. 1c). Additionally, the

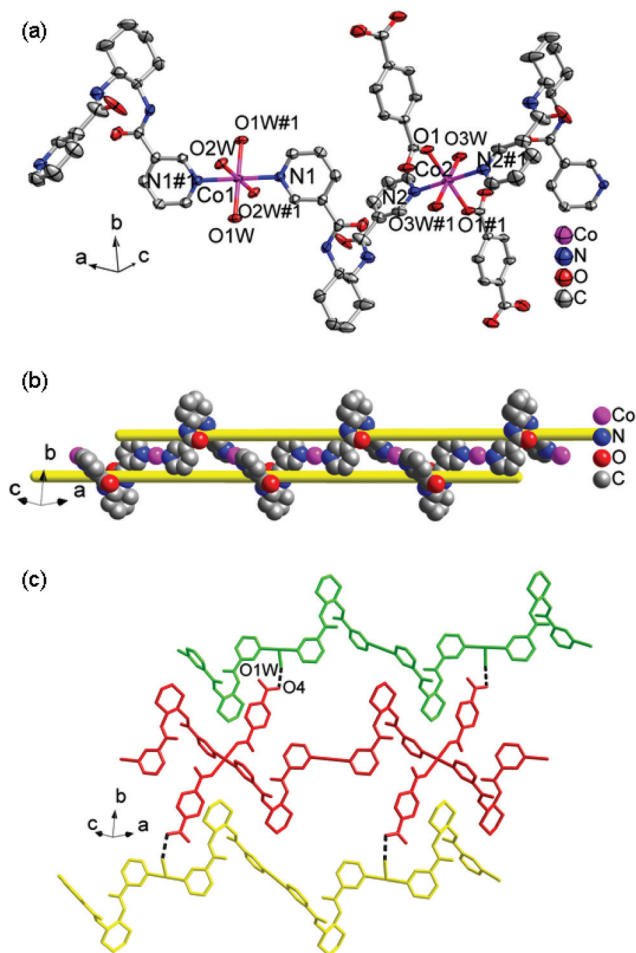


Fig. 1 (a) The coordination environment of the Co(II) ions in complex 1 with 50% thermal ellipsoids. Symmetry codes: #1 $-x + 2, -y + 1, -z - 1$. (b) The 1D $[\text{Co}(\text{3-bpah})_n$ meso-helical chain. (c) A view of the 2D supramolecular layer in complex 1.

$\text{O1W-H1WB}\cdots\text{O2}$ (2.6892 Å) hydrogen-bonding interactions interlink the adjacent layers to form a 3D supramolecular framework (Fig. S2b†). The solvent-accessible voids by PLATON²⁸ calculations are 3.6% for 1 and 3.5% for 2.

[Cu(3-bpah)(1,4-BDC)] (3). Complex 3 crystallizes in the monoclinic space group $C2/c$ with one crystallographically unique Cu(II) ion. The Cu(II) center maintains a quadrilateral coordination environment, as shown in Fig. 2a, and is coordinated by two nitrogen atoms of distinct 3-bpah ligands, and two oxygen atoms from two different 1,4-BDC anions. The lengths of the Cu–N bonds are both 2.000(3) Å, while the Cu–O bonds are 1.947(2) Å. In 3, 1,4-BDC acts as a μ_2 -bridging ligand, with both carboxyl groups of 1,4-BDC adopting the same coordination mode: $\mu_1-\eta^1:\eta^0$ -mode, which interlink the Cu(II) ions to produce a 1D $[\text{Cu}(1,4\text{-BDC})]_n$ chain with a non-bonding Cu \cdots Cu distance of 10.84 Å (Fig. S3†). The 3-bpah ligand adopts a μ_2 -bridging mode and connects the Cu(II) ions $[\text{Cu}\cdots\text{Cu}$ distance: 10.89 Å, Table S7†] to build a 1D $[\text{Cu}(\text{3-bpah})]_n$ meso-helical chain (Fig. 2b), which is similar to that in complex 1. The 1D $[\text{Cu}(1,4\text{-BDC})]_n$ chains and $[\text{Cu}(\text{3-bpah})]_n$

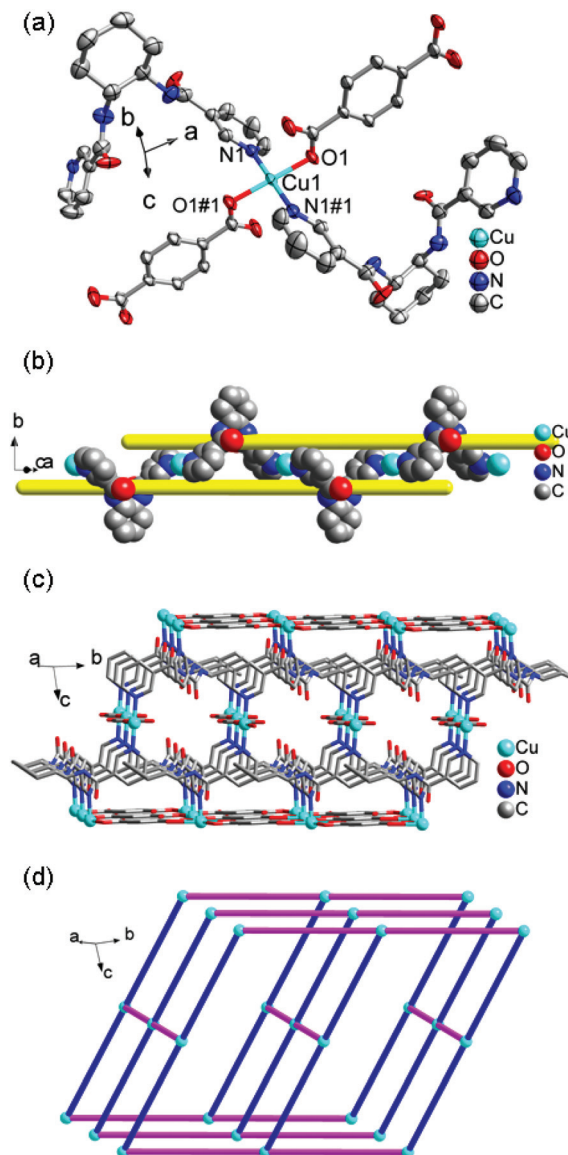


Fig. 2 (a) The coordination environment of the Cu(II) ion in complex 3 with 50% thermal ellipsoids. Symmetry codes: #1 $-x + 1/2, -y + 3/2, -z + 1$. (b) A view of the 1D $[\text{Cu}(\text{3-bpah})]_n$ meso-helical chain in complex 3. (c) A view of the 3D framework in complex 3. (d) A view of the CdSO_4 -like topology of complex 3.

meso-helical chains are further linked by each other to form a 3D framework (Fig. 2c). Topological analysis was carried out to simplify the 3D architecture. The 3-bpah/1,4-BDC is viewed as a linear rod, and the Cu(II) ion could be regarded as a 4-connected node. In such a way, the whole structure illustrates a uninodal 4-connected framework with the Schläfli symbol of $(6^5\cdot 8)$, which is topologically identical to the augmented square CdSO_4 array (Fig. 2d). The PLATON²⁸ calculations show that the largest solvent-accessible void is 10.4%.

[Zn(3-bpah)(1,4-BDC)]·H₂O (4). The single crystal X-ray analysis reveals that 4 is a 2D coordination network formed by Zn(II) ions, 3-bpah ligands and 1,4-BDC anions. Fig. 3a shows the coordination environment of the Zn(II) ion, which is four-

coordinated by two pyridyl nitrogen atoms of two different 3-bpah ligands [$\text{Zn1-N1} = 2.0461(16) \text{ \AA}$, $\text{Zn1-N2} = 2.0755(16) \text{ \AA}$], and two oxygen atoms of two 1,4-BDC anions [$\text{Zn1-O1} = 1.9240(14) \text{ \AA}$, $\text{Zn1-O3} = 1.9465(13) \text{ \AA}$] to give a distorted tetrahedral coordination geometry. In **4**, two μ_2 -bridging 3-bpah ligands through their pyridyl nitrogen atoms (Table S7†) connect two Zn(II) ions to form a $[\text{Zn}_2(3\text{-bpah})_2]$ binuclear subunit with the dimensional size of $14.35 \times 10.40 \text{ \AA}^2$ (Fig. 3b). The 1,4-BDC acts as a bis(monodentate) bridging ligand, with two carboxyl groups adopting the same $\mu_1\text{-}\eta^1\text{:}\eta^0$ -mode to link the Zn(II) ions, constructing a 1D $[\text{Zn}(1,4\text{-BDC})]_n$ zigzag chain with non-bonding $\text{Zn1}\cdots\text{Zn1A}$ and $\text{Zn1A}\cdots\text{Zn1B}$ distances of 10.96 and 10.95 \AA , respectively (Fig. 3c). The adjacent 1D $[\text{Zn}(1,4\text{-BDC})]_n$ zigzag chains are linked by $[\text{Zn}_2(3\text{-bpah})_2]$ binuclear subunits to form a 2D coordination network

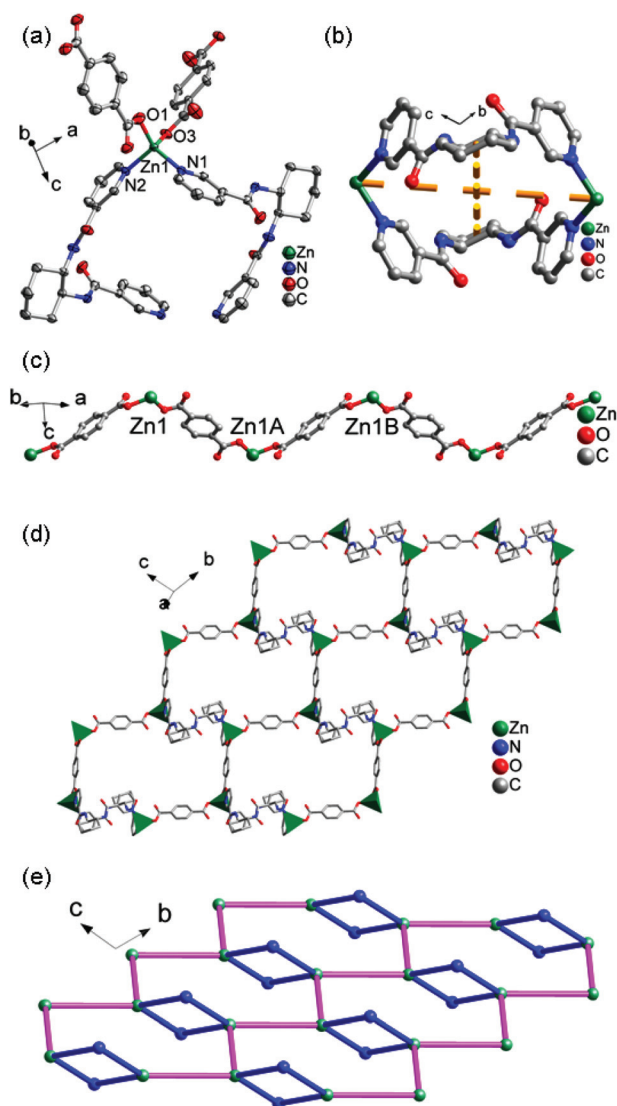


Fig. 3 (a) The coordination environment of the Zn(II) ion in complex **4** with 50% thermal ellipsoids. (b) A view of the $[\text{Zn}_2(3\text{-bpah})_2]$ loop in complex **4**. (c) A view of the 1D zigzag chain in complex **4**. (d) A view of the 2D layer of complex **4**. (e) A view of the 2D (2,4)-connected topology of complex **4**.

(Fig. 3d). In complex **4**, each Zn(II) center acts as a 4-connected node to connect two 3-bpah ligands and two 1,4-BDC anions. The 3-bpah ligands serve as the 2-connected nodes and the 1,4-BDC anions act as linkers. Thus, the topological analysis reveals that complex **4** represents a (2,4)-connected network (Fig. 3e) with the Schläfli symbol $(4\cdot 8^5)(4)$. Finally, the 2D layers are further connected by two kinds of O–H \cdots O hydrogen-bonding interactions to generate a 3D supramolecular framework (Fig. S4†). One hydrogen-bonding interaction is between the carbonyl oxygen atom (O5) of 3-bpah and the oxygen atom (O1W) from the coordinated water molecule with a distance of 3.0119 \AA , and the other is between the carboxyl oxygen atom (O4) of 1,4-BDC and the oxygen atom (O1W) from the coordinated water molecule with a distance of 3.0340 \AA . Moreover, by padding the water molecules into the large porous channels, there is no residual solvent accessible void in the whole structure. After removing the H_2O molecules, the voids are found to be 3.9% in the final network by using PLATON²⁸ calculations.

[Cd(3-bpah)(1,4-BDC)(H₂O)] (**5**). Complex **5** is a 2D Cd(II) coordination framework bridged by organic ligands 3-bpah and 1,4-BDC. The fundamental building unit of **5** contains one Cd(II) ion, one 3-bpah ligand, one 1,4-BDC anion and one coordinated water molecule (Fig. 4a). The Cd(II) center takes a distorted octahedron geometry, in which one nitrogen atom (N1) from the 3-bpah ligand [$\text{Cd(1)-N(1)} = 2.3200(15) \text{ \AA}$] and three oxygen atoms (O1, O3, and O4) from two 1,4-BDC anions [$\text{Cd(1)-O(1)} = 2.2784(16) \text{ \AA}$, $\text{Cd(1)-O(3)} = 2.5293(13) \text{ \AA}$, $\text{Cd(1)-O(4)} = 2.3037(13) \text{ \AA}$] form the equatorial plane. The apical positions are occupied by one amide oxygen atom (O5) from a 3-bpah ligand [$\text{Cd(1)-O(5)} = 2.3538(13) \text{ \AA}$] and one oxygen atom (O1W) from one coordinated water molecule [$\text{Cd(1)-O(1W)} = 2.2925(14) \text{ \AA}$]. Two 3-bpah ligands with a μ_2 -bridging mode (via the ligation of one pyridyl nitrogen and one amide oxygen atom) link two Cd(II) ions to generate a $[\text{Cd}_2(3\text{-bpah})_2]$ binuclear subunit with the dimensional size of $5.30 \times 3.57 \text{ \AA}^2$ (Fig. 4b). The dimensional size of the binuclear subunit in **5** is obviously smaller than that in **4**, which is attributed to the different coordination modes of the 3-bpah ligands (Table S7†). In **5**, the 1,4-BDC anions possess two different coordination modes. One acts as a bis(chelating) bridging ligand linking two Cd(II) ions, in which each carboxyl group adopts a $\mu_1\text{-}\eta^1\text{:}\eta^1$ -mode, while the other acts as a bis(monodentate) bridging ligand, in which each carboxyl group with a $\mu_1\text{-}\eta^1\text{:}\eta^0$ -mode connects two Cd(II) ions. The adjacent Cd(II) ions are bridged by 1,4-BDC anions with different coordination modes to form a 1D $[\text{Cd}(1,4\text{-BDC})]_n$ zigzag chain (Fig. 4c). Such 1D chains are further interlinked by a $[\text{Cd}_2(3\text{-bpah})_2]$ loop to form a 2D layer (Fig. 4d). Topologically, complex **5** displays a 2D (2,4)-connected $(4\cdot 8^5)(4)$ structure, which is similar to that of complex **4** (Fig. 4e). The 2D layers are further linked by hydrogen-bonding interactions between the coordinated water molecules O1W and the carboxyl O atoms of 1,4-BDC [$\text{O(1W)-H(1WA)}\cdots\text{O(2)} = 2.8327 \text{ \AA}$] to generate a 3D supramolecular architecture (Fig. S5†). In addition, the voids are found to be 9.6% in the final networks by using PLATON²⁸ calculations.

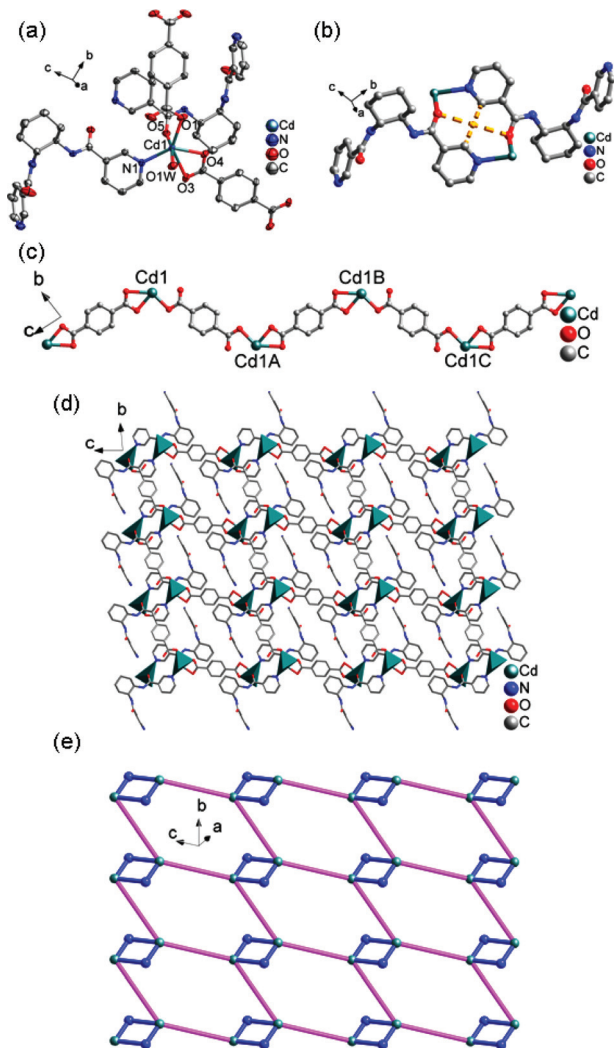


Fig. 4 (a) The coordination environment of the Cd(II) ion in complex 5 with 50% thermal ellipsoids. (b) A view of the $[\text{Cd}_2(3\text{-bpah})_2]$ loop in complex 5. (c) A view of the 1D zigzag chain in complex 5. (d) A view of the 2D layer of complex 5. (e) A view of the 2D (2,4)-connected topology in complex 5.

It is well known that the central metal ions play an important role in the formation of the final frameworks and various structures. In this work, five coordination polymers based on 3-bpah and 1,4-BDC mixed ligands and different metal centers (Co(II), Ni(II), Cu(II), Zn(II), Cd(II)) have been synthesized under similar hydrothermal conditions, which exhibit distinct coordination networks. In complexes 1 and 2 the Co(II)/Ni(II) ions, which belong to the VIII B group and have similar atomic radii, were used as the central metals and showed a coordination number of 6. As a result, isostructural 1D chains 1 and 2 have been obtained, in which the 3-bpah ligands act as μ_2 -bridging ligands to connect the Co(II)/Ni(II) ions yielding a 1D *meso*-helical chain with monodentate 1,4-BDC ligands at both sides in an outward fashion. When the Cu(II) ions were selected as the central metal in 3, a 3D CdSO_4 framework was formed, in which the Cu(II) ions exhibited the coordination number of 4, both the 3-bpah and 1,4-BDC ligands act as

μ_2 -bridging ligands to link the Cu(II) ions producing two kinds of 1D chains. In complex 4, the Zn(II) ions also show the coordination number of 4 and the 1,4-BDC ligands also act as μ_2 -bridging ligands, however, a 2D network was constructed. The 3-bpah ligands adopt a μ_2 -bridging mode (*via* ligation of two pyridyl nitrogen atoms) to connect two Zn(II) ions constructing a $[\text{Zn}_2(3\text{-bpah})_2]$ binuclear subunit but not a 1D chain, which is different from that in 1–3. When the Cd(II) ions, which belong to the same IIB group as the Zn(II) ions but have a bigger atomic radius, were employed as the central metal in complex 5, the coordination number of the Cd(II) ions was 6. In addition, though complex 5 shows a similar 2D network to 4, the 3-bpah ligands adopt a different μ_2 -bridging mode (*via* the ligation of one pyridyl nitrogen and one amide oxygen atom) to link two Cd(II) ions constructing a smaller $[\text{Cd}_2(3\text{-bpah})_2]$ binuclear subunit. It is the central metal that determines the final structure of complexes 1–5, as well as the influence the coordination modes of the 3-bpah and 1,4-BDC ligands. The differences in the coordination numbers and the atomic radii of the central metal ions are the key reasons for producing diverse structures. In addition, the 3-bpah ligands act as μ_2 -bridging ligands in complexes 1–5 but exhibit different conformations and coordination modes, resulting in the formation of different metal-3-bpah subunits, which indicates that the semi-rigid 3-bpah is an excellent structural constructor to design and build novel complexes.

IR spectra

The IR spectra of complexes 1–5 are shown in Fig. S6.† The bands at 3300, 3299, 3280 and 3412 cm^{-1} are assigned to the stretching and bending vibrations of the –OH groups of water molecules for complexes 1, 2, 4 and 5, respectively.^{29,30} The strong peaks at 1649, 1649, 1651, 1656 and 1652 cm^{-1} for complexes 1–5 are identified as the $\nu_{\text{C=O}}$ vibrations of the amide groups.^{29–31} The presence of the characteristic bands at 1598 and 1422 cm^{-1} for 1, 1599 and 1422 cm^{-1} for 2, 1607 and 1431 cm^{-1} for 3, 1601 and 1428 cm^{-1} for 4 and 1624 and 1433 cm^{-1} for 5, may be attributed to the asymmetric and symmetric vibrations of the carboxyl groups.^{29–31} The strong peaks at 1364 and 1053 cm^{-1} for 1, 1365 and 1050 cm^{-1} for 2, 1369 and 1016 cm^{-1} for 3, 1382 and 1054 cm^{-1} for 4 and 1367 and 1018 cm^{-1} for 5, suggest the $\nu_{\text{C-N}}$ stretching vibrations of the pyridyl ring of the 3-bpah ligands.^{29–31}

Powder X-ray diffraction and thermogravimetric analyses

The powder X-ray diffraction (PXRD) patterns for complexes 1–5 are presented in Fig. S7.† The as-synthesized patterns are in good agreement with the corresponding simulated ones, indicating the phase purity of the samples.

Thermogravimetric analysis was carried out for complexes 1–5 in order to investigate their thermal stability. As shown in Fig. S8,† the first weight loss of 8.72% for 1, 8.49% for 2, 2.98% for 4 and 2.88% for 5, occurred in the range of 151–195 °C, 136–206 °C, 52–118 °C and 117–173 °C, respectively, and can be attributed to the removal of water molecules (calcd 8.98% for 1, 8.98% for 2, 3.15% for 4 and 2.91% for 5).

Then, the second weight loss of about 78.75%, 79.23%, 82.36% and 76.18% (calcd 78.55%, 78.55%, 82.69% and 76.41%) in the range of 251–684 °C, 262–511 °C, 311–639 °C and 384–567 °C, may suggest the decomposition of the organic ligands. Complex 3 does not contain water molecules, and it is stable up to 205 °C, after which the framework begins to decompose with a continuous weight loss of 85.27% up to 620 °C, which could be attributed to the loss of the organic ligands (calcd 85.51%). For the five complexes, the final residues of 12.53%, 12.28%, 14.73%, 14.66% and 20.94% are close to the calculated values of 12.47%, 12.47%, 14.49%, 14.16% and 20.68% by assuming the CoO, NiO, CuO, ZnO and CdO phases as the final residues, respectively.

Fluorescence property

The fluorescence properties of the transition metal complexes 1–5, together with the free 3-bpah ligand were studied in the solid-state at room temperature. The emission spectra of the complexes and the free ligand have been measured under the same conditions (slit width = 2.5 nm) and are depicted in Fig. 5. Obviously, the free ligand 3-bpah exhibits the emission peaks at 386 nm with the excitation at 315 nm, which can probably be assigned to the $\pi \rightarrow \pi^*$ or $n \rightarrow \pi^*$ transitions.^{32,33} The fluorescence peaks at about 386 nm for 1–3, 420 nm for 4 and 424 nm for 5 are found in the emission spectra when they are excited at 320 nm, respectively. It was considered that the 1,4-BDC anion has no significant contribution to the fluorescence emission of the coordination polymers with the presence of the N-donor ligands.^{34,35} Although the Co(II)/Ni(II)/Cu(II) complexes do not contain d^{10} metal centers, a series of weak fluorescence Co(II)/Ni(II)/Cu(II) complexes have been reported.^{34–36} Here, complexes 1–3 also show weak fluorescence bands. The density functional theory calculations indicate that the weak fluorescence may be a ligand-based emission, which may be ascribed to the $\pi \rightarrow \pi^*$ or $n \rightarrow \pi^*$ transitions.¹⁸ For complexes 4 and 5, it is clear that an obvious red-shifted (34 nm for 4 and 38 nm for 5) strong emission

band has been observed compared with the free 3-bpah ligand. The fluorescence behaviors of 4 and 5 can be best ascribed to the ligand-to-metal charge-transfer (LMCT).^{18,37}

In order to investigate the effect of the guest molecules on the fluorescence properties, the fluorescence spectra of the powder samples of 4a and 5a (the guest-free form of 4 and 5) were recorded. Desolvated 4a and 5a were prepared as follows: after immersion in CH₃OH for 3 days with the soaking solution being replaced every 6 h, the solvent-exchanged samples were evacuated at 60 °C for 1 h and then 120 °C for over 3 h. Interestingly, the fluorescence spectrum of 4a reveals an obvious fluorescence enhancement as shown in Fig. S9,† which indicates that the guest water molecules in 4 have a great effect on the fluorescence intensity. The fluorescence spectrum of 5a is same as that of 5, indicating that there are no guest molecules in the voids of network 5, which is consistent with the formula of 5. In order to further confirm the effect of the guest molecules on the fluorescence properties, the solid-state fluorescence properties of 4a and 5a containing various solvent molecules (designated as 4a-solvent and 5a-solvent, respectively) were investigated at room temperature. The complexes 4a-solvent and 5a-solvent were prepared by introducing 5.0 mg of 4a and 5a fine powder into 5.0 mL of MeOH, EtOH, CH₃CN, CH₂Cl₂, DMF, DMSO, THF, distilled water, diethyl ether or cyclohexane for 72 h, respectively. After sonication treatment, aging for over 24 h, shaking, filtering and drying in air, the fluorescence samples were obtained. Then the fluorescence spectra were measured.

As shown in Fig. 6 and Fig. S10,† the fluorescence intensity of 4a-EtOH was enhanced. In contrast, for the other 4a-solvent, such as MeOH, CH₃CN, CH₂Cl₂, DMF, DMSO, distilled water, diethyl ether and cyclohexane, different degrees of a decrease in the fluorescence properties can be observed. Furthermore, there was no obvious change for 4a-THF. However, for 5a-MeOH, EtOH, CH₃CN and CH₂Cl₂, the fluorescence intensities were enhanced; for 5a-DMSO, no fluorescence intensity change could be observed; while the other 5a-solvents show different degrees of a fluorescence intensity decrease. The results indicate that the guest solvent molecules in the voids of network 4a or 5a exhibit a great effect on their fluorescence intensity. The fluorescence response of 4a-EtOH and 5a-EtOH was the largest, while the fluorescence intensity of 4a-cyclohexane and 5a-cyclohexane was the lowest.

The above results show that 4a and 5a may be applied as fluorescence sensors for some organic molecules with a high sensitivity and selectivity. Specifically, an amount of ethanol can be easily sensed because of its significant fluorescence enhancement, which is dependent on its content. Fig. S11† shows the fluorescence spectra of 4a-EtOH–H₂O and 5a-EtOH–H₂O with various amounts of ethanol. It can be clearly seen that the fluorescence intensity gradually increase with the increase of the ethanol content, which indicates that 4a and 5a are promising fluorescent probes for detecting both EtOH molecules and water molecules simultaneously.

In addition, we also investigated the solid-state fluorescence properties of the 4a- and 5a-aromatic molecules, which

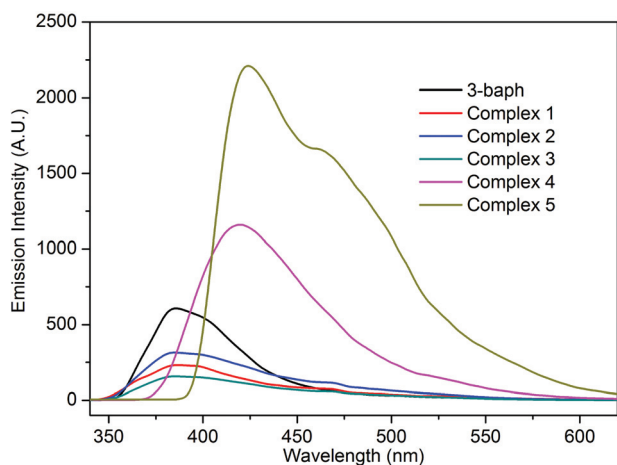


Fig. 5 The emission spectra of complexes 1–5 and the free ligand 3-bpah.

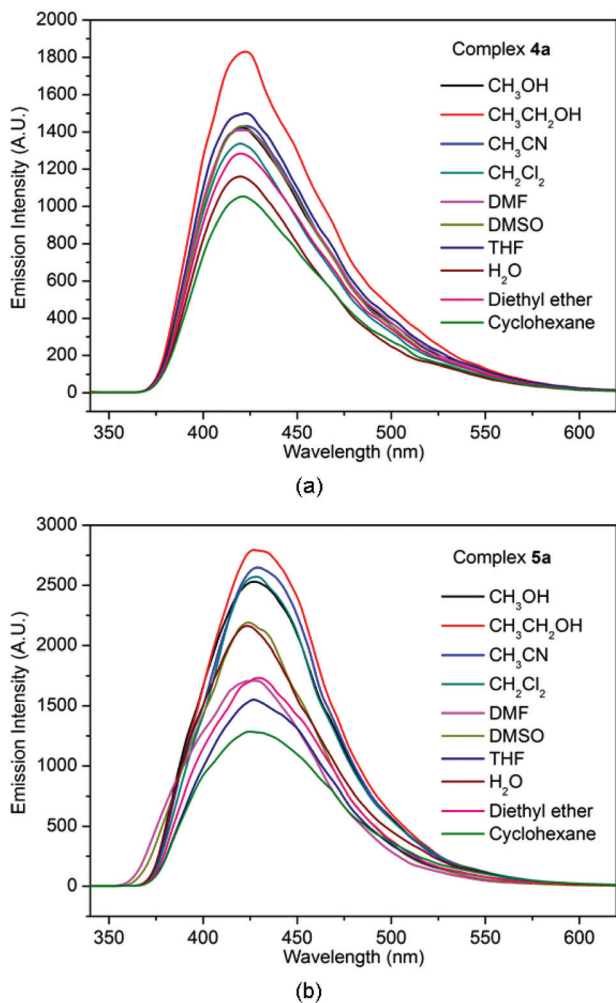


Fig. 6 The solid-state fluorescence spectra of complexes **4a**-solvent and **5a**-solvent.

revealed a unique fluorescence enhancement and quenching behavior upon immersing in methylbenzene, benzene and nitrobenzene, respectively (Fig. 7). Among them, methylbenzene enhanced the emission intensity most significantly (60.6% for **4a** and 78.9% for **5a**), followed by benzene (54.4% for **4a** and 49.5% for **5a**). Oppositely, nitrobenzene is a fluorescence quencher, which quenched the emission intensity as much as 81.8% for **4a** and 95.9% for **5a**. This is in accordance with the trend of the electron-withdrawing groups. The results demonstrate the ability of **4a** and **5a** as fluorescence sensors to detect some aromatic molecules. As shown in Fig. 8, with the increase of the nitrobenzene content, the emission intensity of **4a**- and **5a**-nitrobenzene-ethanol decreases gradually, which indicates that **4a** and **5a** are promising fluorescent probes for detecting both nitrobenzene and ethanol simultaneously.

Electrochemical properties

The electrochemical studies of 1-CPE, 2-CPE and 3-CPE were carried out in a 0.01 M H_2SO_4 + 0.5 M Na_2SO_4 aqueous solution. Fig. 9 and Fig. S12[†] show the cyclic voltammograms of

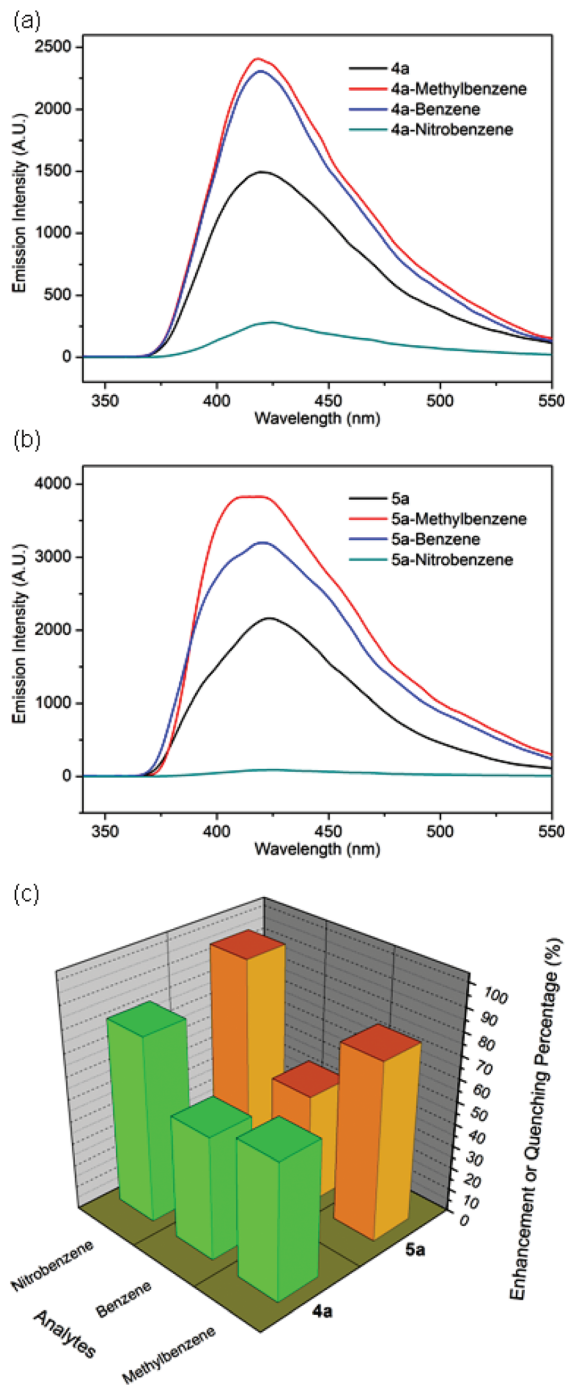


Fig. 7 (a, b) The solid-state fluorescence spectra of **4a** and **5a**, as well as **4a**- and **5a**-methylbenzene, benzene and nitrobenzene. (c) A view of the percentage of fluorescence enhancement and quenching of **4a** and **5a** by three different analytes.

1-3-CPE at different scan rates, respectively. It can be seen clearly that in the potential range of 650 to 150 mV, 800 to -100 mV and 400 to -600 mV, a quasi-reversible redox peak is observed at the 1-3-CPE, respectively, which could be attributed to the redox couple of $\text{Co}^{\text{III}}/\text{Co}^{\text{II}}$, $\text{Ni}^{\text{III}}/\text{Ni}^{\text{II}}$ and $\text{Cu}^{\text{II}}/\text{Cu}^{\text{I}}$, respectively.^{18,19} The mean peak potentials $E_{1/2} = (E_{\text{pa}} + E_{\text{pc}})/2$

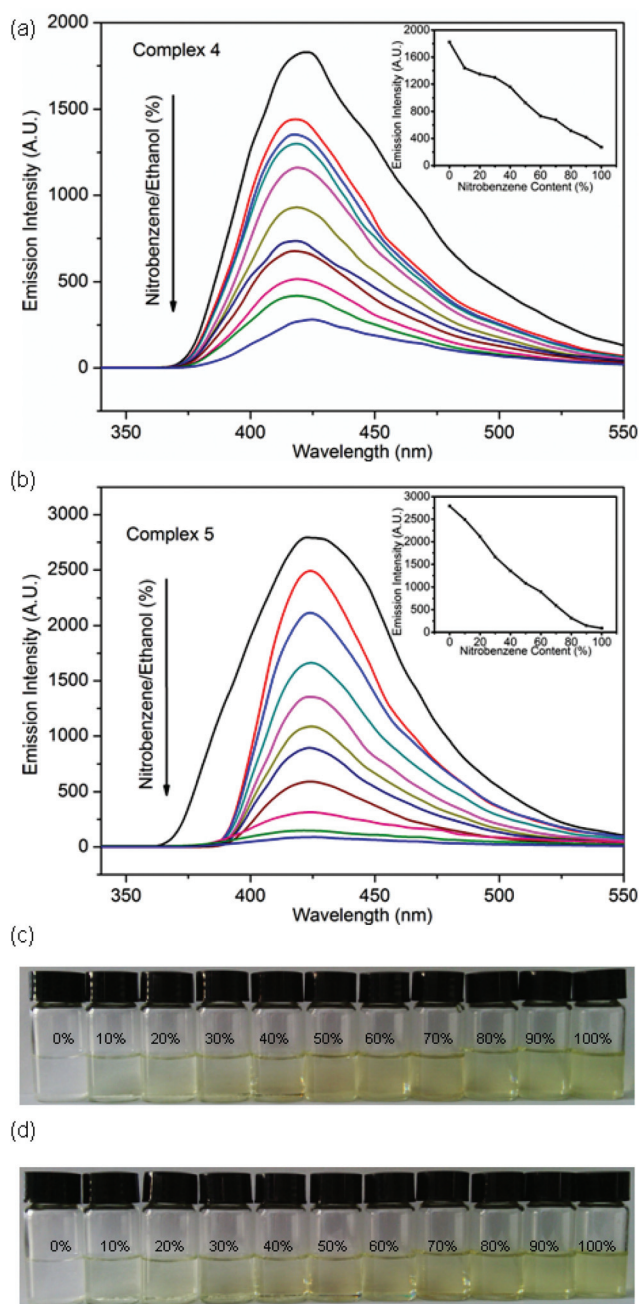


Fig. 8 The solid-state fluorescence spectra of **4a** (a) and **5a** (b) immersed in ethanol in the presence of various amounts of nitrobenzene (the insert is graph of the fluorescence intensity of **4a** and **5a** ethanol as a function of the nitrobenzene content). The photographs show **4a** (c) and **5a** (d) immersed in different ratios of nitrobenzene/ethanol.

are +378 mV for **1**-CPE, +326 mV for **2**-CPE, and -30 mV for **3**-CPE (50 mV s^{-1}), respectively.

The effect of the scan rates on the electrochemical behavior of **1**–**3**-CPE can be seen from Fig. 9 and Fig. S12,[†] with the scan rates increasing from 10 to 100 mV s^{-1} , the peak potentials of **1**–**3**-CPE change gradually: the cathodic peak potentials shift to the negative direction and the corresponding anodic

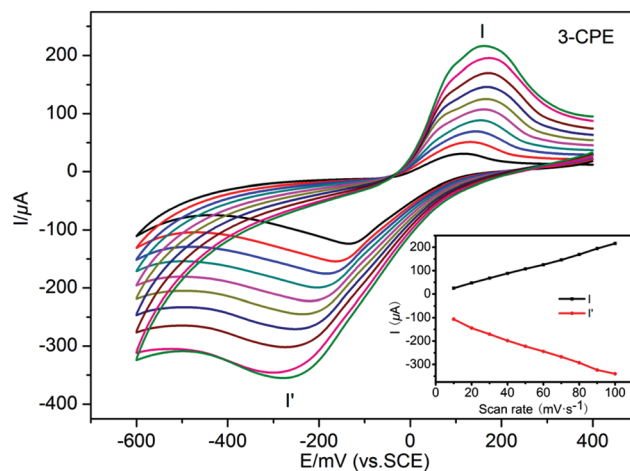


Fig. 9 The cyclic voltammograms of **3**-CPE in a $0.01 \text{ M H}_2\text{SO}_4 + 0.5 \text{ M Na}_2\text{SO}_4$ aqueous solution at different scan rates (from inner to outer: 10, 20, 30, 40, 50, 60, 70, 80, 90 and 100 mV s^{-1}). The inset shows the plots of the anodic and cathodic peak currents against the scan rates.

peak potentials shift to the positive direction. The plots of the peak current *versus* scan rate are shown in the inset of Fig. 9 and Fig. S12.[†] The anodic and cathodic peak currents are proportional to the scan rates, indicating that the redox processes for **1**–**3**-CPE are surface-controlled.^{16,26}

In addition, we investigated the electrocatalytic activity of **1**–**3**-CPE toward the reduction of nitrite. No obvious response on a bare CPE in a $0.01 \text{ M H}_2\text{SO}_4 + 0.5 \text{ M Na}_2\text{SO}_4$ aqueous solution containing a $1.0 \text{ mmol L}^{-1} \text{ KNO}_2$ solution can be observed in the potential ranges of 650 to 150 mV for **1**, 800 to -100 mV for **2** and 400 to -600 mV for **3**. As shown in Fig. 10 and Fig. S13,[†] with the addition of nitrite, the reduction peak currents of the **1**–**3**-CPEs increase while the corresponding oxidation peak currents decrease, which indicates that the

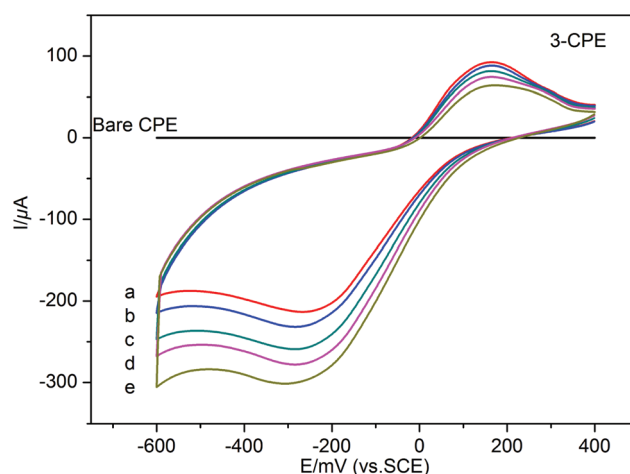


Fig. 10 The cyclic voltammograms of the bare CPE in a $0.01 \text{ M H}_2\text{SO}_4 + 0.5 \text{ M Na}_2\text{SO}_4$ aqueous solution containing $1.0 \text{ mmol L}^{-1} \text{ KNO}_2$, **3**-CPE in a $0.01 \text{ M H}_2\text{SO}_4 + 0.5 \text{ M Na}_2\text{SO}_4$ aqueous solution containing: 0.0 (a), 2.0 (b), 4.0 (c), 6.0 (d) and 8.0 (e) $\text{mmol L}^{-1} \text{ KNO}_2$, respectively. Scan rate: 50 mV s^{-1} .

1–3-CPEs have an electrocatalytic activity toward the reduction of nitrite.

Although the electrochemical behaviors of some MOCs based on Co(II)/Ni(II)/Cu(II) ions have been reported, their electrochemical properties are different.^{16,38} Mukherjee *et al.*¹⁶ reported the electrochemical behaviors of a series of Co(II), Ni(II) and Cu(II) complexes with a hexadentate pyridine amide ligand, in which the Co(II)/Ni(II)/Cu(II) complexes revealed a one-electron quasi-reversible Co^{III}–Co^{II}/Ni^{III}–Ni^{II}/Cu^{II}–Cu^I response with $E_{1/2} = 0.48/1.17/-0.88$ V in CH₂Cl₂ (0.1 M in TBAP) at a platinum electrode, respectively. The differences of the mean peak potential among the corresponding transition metal complexes may be ascribed to the different electrolyte solutions. In addition, our group³⁸ have also obtained three isostructural Co(II)/Ni(II)/Cu(II) coordination polymers, which exhibited a reversible redox peak, respectively. Unfortunately, they have no electrocatalytic activity toward the reduction of nitrite.

Conclusion

In summary, we have successfully synthesized five new metal-organic coordination polymers based on five metal(II) ions and the mixed ligands of semi-rigid bis-pyridyl-bis-amide ligand 3-bpah and 1,4-BDC. The diverse structures of the title complexes indicate that the central metal ions play an important role in the construction of the final framework. Complexes 4 and 5 exhibit excellent fluorescence properties and fluorescent sensing behaviors toward ethanol and nitrobenzene. The central metals also show great effects on the various properties of the target complexes. Moreover, the fluorescence selectivity of 4 and 5 make them promising candidates for use as fluorescent sensor materials.

Acknowledgements

The support of the National Natural Science Foundation of China (no. 20871022, 21171025), New Century Excellent Talents in University (NCET-09-0853) and Program of Innovative Research Team in University of Liaoning Province (LT2012020) is gratefully acknowledged.

References

- O. M. Yaghi, M. O'Keeffe, N. W. Ockwig, H. K. Chae, M. Eddaoudi and J. Kim, *Nature*, 2003, **423**, 705.
- T. Uemura, N. Uchida, A. Asano, A. Saeki, S. Seki, M. Tsujimoto, S. Isoda and S. Kitagawa, *J. Am. Chem. Soc.*, 2012, **134**, 8360.
- V. N. Vukotic and S. Loeb, *Chem. Soc. Rev.*, 2012, **41**, 5896.
- J. Zhang, S. M. Chen, T. Wu, P. Y. Feng and X. H. Bu, *J. Am. Chem. Soc.*, 2008, **130**, 12882.
- G. Y. Wang, L. L. Yang, Y. Li, H. Song, W. J. Ruan, Z. Chang and X. H. Bu, *Dalton Trans.*, 2013, **42**, 12865.
- E. Ribeiro and Y. Gushikem, *Electroanalysis*, 1999, **11**, 1280.
- A. Dhakshinamoorthy and H. Garcia, *Chem. Soc. Rev.*, 2012, **41**, 5262.
- Y. B. Huang, T. F. Liu, J. X. Lin, J. Lü, Z. J. Lin and R. Cao, *Inorg. Chem.*, 2011, **50**, 2191.
- Y. B. Huang, T. Ma, P. Huang, D. S. Wu, Z. J. Lin and R. Cao, *ChemCatChem*, 2013, **5**, 1877.
- Y. B. Huang, S. J. Liu, Z. J. Lin, W. J. Li, X. F. Li and R. Cao, *J. Catal.*, 2012, **292**, 111.
- N. Chilton, S. Langley, B. Moubaraki, A. Soncini, S. Battena and K. Murray, *Chem. Sci.*, 2013, **4**, 1719.
- C. H. Lee, H. Y. Huang, Y. H. Liu, T. T. Luo, G. H. Lee, S. M. Peng, J. C. Jiang, I. Chao and K. L. Lu, *Inorg. Chem.*, 2013, **52**, 3962.
- S. J. Liu, Y. B. Huang, Z. J. Lin, X. F. Li and R. Cao, *RSC Adv.*, 2013, **3**, 9279.
- C. Yan, K. Li, S. C. Wei, H. P. Wang, L. Fu, M. Pan and C. Y. Su, *J. Mater. Chem.*, 2012, **22**, 9846.
- S. L. Huang, X. X. Li, X. J. Shi, H. W. Hou and Y. T. Fan, *J. Mater. Chem.*, 2010, **20**, 5695.
- S. Pandey, P. P. Das, A. K. Singh and R. Mukherjee, *Dalton Trans.*, 2011, **40**, 10758.
- T. Mitkina, N. Zakharchuk, D. Naumov, O. Gerasko, D. Fenske and V. Fedin, *Inorg. Chem.*, 2008, **47**, 6748.
- Y. J. Cui, Y. F. Yue, G. D. Qian and B. L. Chen, *Chem. Rev.*, 2012, **112**, 1126.
- Y. C. Chang and S. L. Wang, *J. Am. Chem. Soc.*, 2012, **134**, 9848.
- G. L. Liu, Y. J. Qin, L. Jing, G. Y. Wei and H. Li, *Chem. Commun.*, 2013, **49**, 1699.
- A. Benvidi, P. Kakoolaki, A. Gorji, M. Mazloum-Ardakani, H. Zare and R. Vafazadeh, *Anal. Methods*, 2013, **5**, 6649.
- X. L. Wang, H. Y. Lin, B. Mu, A. X. Tian and G. C. Liu, *Dalton Trans.*, 2010, **39**, 6187.
- X. L. Wang, J. Luan, H. Y. Lin, C. Xu, G. C. Liu, J. W. Zhang and A. X. Tian, *CrystEngComm*, 2013, **15**, 9995.
- X. L. Wang, J. Luan, H. Y. Lin, Q. L. Lu, C. Xu and G. C. Liu, *Dalton Trans.*, 2013, **42**, 8375.
- H. Chen, H. Y. An, X. Liu, H. L. Wang, Z. F. Chen, H. Zhang and Y. Hu, *Inorg. Chem. Commun.*, 2012, **21**, 65.
- G. M. Sheldrick, *Acta Crystallogr., Sect. A: Found. Crystallogr.*, 2008, **64**, 112.
- X. L. Wang, H. Y. Zhao, H. Y. Lin, G. C. Liu, J. N. Fang and B. K. Chen, *Electroanalysis*, 2008, **20**, 1055.
- A. L. Spek, *PLATON, A Multipurpose Crystallographic Tool*, Utrecht University, Utrecht, The Netherlands, 2001.
- P. S. Kalsi, *Spectroscopy Of Organic Compounds*, New Age International, New Delhi, 2008.
- L. J. Bellamy, *The Infrared Spectra of Complex Molecules*, Wiley, New York, 1958.
- B. Dolenský, R. Konvalinka, M. Jakubek and V. Král, *J. Mol. Struct.*, 2013, **1035**, 124.
- Y. Gong, J. Li, J. B. Qin, T. Wu, R. Cao and J. H. Li, *Cryst. Growth Des.*, 2011, **11**, 1662.

- 33 M. J. Sie, Y. J. Chang, P. W. Cheng, P. T. Kuo, C. W. Yeh, C. F. Cheng, J. D. Chen and J. C. Wang, *CrystEngComm*, 2012, **14**, 5505.
- 34 Y. Bai, G. J. He, Y. G. Zhao, C. Y. Duan, D. B. Dang and Q. J. Meng, *Chem. Commun.*, 2006, 1530.
- 35 J. P. Zou, Q. Peng, Z. H. Wen, G. S. Zeng, Q. J. Xing and G. C. Guo, *Cryst. Growth Des.*, 2010, **10**, 2613.
- 36 S. S. Xiong, S. J. Wang, X. J. Tang and Z. Y. Wang, *CrystEngComm*, 2011, **13**, 1646.
- 37 P. C. Cheng, P. T. Kuo, Y. H. Liao, M. Y. Xie, W. Hsu and J. D. Chen, *Cryst. Growth Des.*, 2013, **13**, 623.
- 38 X. L. Wang, J. Luan, H. Y. Lin, C. Xu and G. C. Liu, *Inorg. Chim. Acta*, 2013, **408**, 139.